VIP Dye-Sensitized Solar Cells

DOI: 10.1002/anie.200704919

Aggregation of ZnO Nanocrystallites for High Conversion Efficiency in Dye-Sensitized Solar Cells**

*Qifeng Zhang, Tammy P. Chou, Bryan Russo, Samson A. Jenekhe, and Guozhong Cao**

As a relatively new class of photovoltaic devices with a photoelectrochemical system consisting of a dye-sensitized semiconductor film and an electrolyte, dye-sensitized solar cells (DSSCs) have been regarded as a promising alternative to conventional solid-state semiconductor solar cells. They are relatively cost-effective, are easy to manufacture, and can be readily shaped with flexible substrates to satisfy the demands of various applications.[1,2] A very important feature of DSSCs is the photoelectrode, which includes mesoporous wide-band-gap oxide semiconductor films with an enormous internal surface area, typically a thousand times larger than that of bulk films.[3–5] To date, the highest solar-to-electric conversion efficiency of over 11% has been achieved with films that consist of 20-nm TiO_2 nanocrystallites sensitized by ruthenium-based dyes.[6] However, further improving the energy conversion efficiency of DSSCs remains a challenge.

Competition between the generation and recombination of photoexcited carriers in DSSCs is a main bottleneck for developing higher conversion efficiency.[6] One possible solution is to use one-dimensional nanostructures that are able to provide a direct pathway for the rapid collection of photogenerated electrons and, therefore, reduce the degree of charge recombination.[7–10] However, such one-dimensional nanostructures seem to have insufficient internal surface area, which limits their energy conversion efficiency at a relatively low level, for example, 1.5% for ZnO nanowires[7] and 4.7% for TiO_2 nanotubes.[9] Another way to increase efficiency is to increase the light-harvesting capability of the photoelectrode film by utilizing optical enhancement effects, which can be achieved by means of light scattering by introducing scatterers into the photoelectrode film. Usami,[11] Ferber and Luther,[12] and Rothenberger et al.[13] have demonstrated theoretically that optical absorption by TiO_2 nanocrystalline films can be promoted by additionally admixing large TiO_2 particles in an optimal volume ratio. This idea was verified experimentally when TiO_2 nanocrystalline films were combined with large SiO_2, Al_2O_3, or TiO_2 particles.[14–17] By coupling a photonic crystal layer to conventional TiO_2 nanocrystalline films as the light scatterer, Nishimura et al.[18] and Halaoui et al.[19] also succeeded in enhancing the light-harvesting capability of solar-cell photoelectrodes. However, the drawback is that the introduction of larger particles into nanocrystalline films will unavoidably lower the internal surface area of the photoelectrode film and, therefore, counteract the enhancement effect of light scattering on the optical absorption, whereas the incorporation of a layer of TiO_2 photonic crystal may lead to an undesirable increase in the electron diffusion length and, consequently, increase the recombination rate of photogenerated carriers.

Herein we report hierarchically structured ZnO films as the photoelectrodes in DSSCs for the enhancement of energy conversion efficiency. The films are comprised of polydisperse ZnO aggregates consisting of nanosized crystallites. The aggregates are submicrometer-sized and, thus, can function as efficient light scatterers, while the nanocrystallites provide the films with the necessary mesoporous structure and large internal surface area. An overall energy conversion efficiency up to 5.4% has been achieved from the film including polydisperse ZnO aggregates, much higher than 1.5–2.4% for ZnO nanocrystalline films,[20–22] 0.5–1.5% for ZnO nanowire films,[7,8,23] and 2.7–3.5% for uniform ZnO aggregate films.[24,25]

Polydisperse ZnO aggregates were synthesized by the hydrolysis of zinc salt in polyol medium at 160°C, similar to the method reported by Jezequel et al.[26] Rapid heating at a rate of 10°C min^{-1} was intentionally used to obtain polydisperse aggregates, that is, with a relatively wide size distribution. The resulting colloidal dispersion was drop-cast onto a fluorine-doped tin oxide (FTO) coated glass substrate to form a film of approximately 9 μm in thickness, and the film was subsequently annealed at 350°C for 1 h in air to remove residual solvents and any organic compounds as well as to improve the contact between the film and the substrate and the connection between the nanocrystallites and between the aggregates. Figure 1 shows the scanning electron microscopy (SEM) images of ZnO film with polydisperse aggregates and a schematic illustration showing the structure of an aggregate. Figure 1a indicates that the film is well stacked with submicrometer-sized ZnO aggregates. Figure 1b presents the highly disordered structure of the film assembled by polydisperse ZnO aggregates with diameters ranging from several tens to several hundreds of nanometers. Figure 1c is a magnified SEM image of an individual ZnO aggregate, revealing that the ZnO aggregate is nearly spherical in

[*] Dr. Q. F. Zhang, Dr. T. P. Chou, B. Russo, Prof. G. Z. Cao
Department of Materials Science and Engineering
University of Washington
Seattle, WA 98195 (USA)
Fax: (+1) 206-543-3100
E-mail: gzcao@u.washington.edu
Homepage: http://depts.washington.edu/solgel/
Prof. S. A. Jenekhe
Department of Chemical Engineering
University of Washington
Seattle, WA 98195 (USA)

[**] This work was financially supported by National Science Foundation, US Department of Energy, Washington Technology Centre, and Air Force Office of Scientific Research.

Supporting information for this article is available on the WWW under http://www.angewandte.org or from the author.

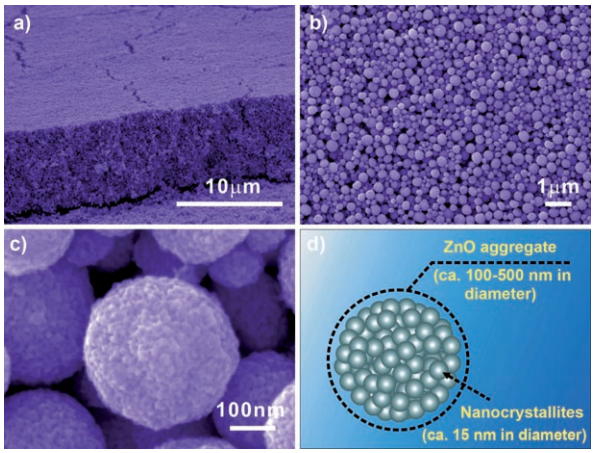

Figure 1. Morphology and structure of the ZnO aggregate film. a) SEM image of the cross section of the ZnO aggregate film. b) SEM image of the top view of the ZnO film consisting of polydisperse aggregates. c) A magnified SEM image of an individual ZnO aggregate. d) A schematic diagram that illustrates the microstructure of aggregated ZnO comprising closely packed nanocrystallites.

shape and consists of packed nanocrystallites. The geometrical structure of an individual aggregate is further schematically illustrated in Figure 1d to demonstrate the porous features provided by the aggregation of nanosized crystallites. This ZnO film has a hierarchical structure, which stems from the combined architecture of the film formed by secondary aggregates with primary nanocrystallites. The sample synthesized at 160 °C is denoted sample 1.

In addition to sample 1, three more ZnO films (samples 2, 3, and 4) with different morphology were prepared at 170, 180, and 190 °C, respectively. Figure 2 shows typical SEM images of these three samples, revealing the gradual degradation in the degree of spherical aggregation of nanocrystallites with increasing synthesis temperature. Sample 2, synthesized at 170 °C, is similar to sample 1 and consists of aggregated ZnO nanocrystallites, but sample 2 shows a slight destruction of the spherical shape (Figure 2a). Sample 3, synthesized at 180 °C (Figure 2b), consists of partial aggregates. It is clear that in sample 3, most of the aggregates have lost their spherical shape. As the synthesis temperature increases further to 190 °C, the obtained ZnO film (sample 4, Figure 2c) only presents the primary nanocrystallites without any aggregation.

X-ray diffraction (XRD) analysis revealed that all four ZnO films had the hexagonal wurtzite structure, despite the different synthesis temperatures and morphologies. The primary nanocrystallite size estimated from the full width at half maximum of the (101) peak using the Scherrer equation revealed that the ZnO nanocrystallites were 15 nm in diameter, and there was no appreciable difference in nanocrystallite size for all the samples regardless of the various morphologies observed by SEM. Nitrogen sorption isotherms were employed to analyze the surface area of the ZnO powder samples. All four samples showed a specific surface area of $80 \pm 2\ m^2 g^{-1}$.

The ruthenium complex *cis*-$[RuL_2(NCS)_2]$ (L = 4,4′-dicarboxy-2,2′-bipyridine), known as N3 dye, was used to sensitize the ZnO films. The sensitization was achieved by immersing the films in a 0.5 mM ethanol solution of N3 dye for approximately 20 min; this immersion time was chosen to avoid the dissolution of surface Zn atoms and formation of Zn^{2+}/dye complexes, which was believed to be harmful to the charge transport from the dye to the semiconductor.[27,28]

As-prepared ZnO solar cells were characterized by measuring the current–voltage behavior while the cells were irradiated by AM 1.5 simulated sunlight with a power density of 100 mW cm^{-2}. Figure 3 shows typical current density versus voltage curves of the four ZnO samples. Sample 1, with near-perfect aggregation, achieved the highest short-circuit current density and, thus, the highest conversion efficiency, whereas sample 4, consisting of only ZnO nanocrystallites, presented the lowest current density and the lowest energy conversion efficiency among all four samples. Table 1 summarizes the open-circuit voltages, the short-circuit current densities, the fill factors, and the overall energy conversion efficiencies for all four samples. All samples possessed the same or similar open-circuit voltages of approximately 600 mV; however, the short-circuit current density varied significantly from 19 mA cm^{-2} for sample 1 to 10 mA cm^{-2} for sample 4. As a result, the energy conversion efficiency varied systematically from 5.4% for sample 1 to 2.4% for sample 4, decreasing as the degree of spherical aggregation decreased.

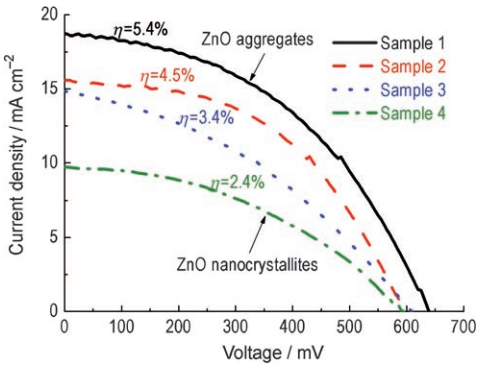

Figure 3. A comparison of photovoltaic behaviors of samples 1–4.

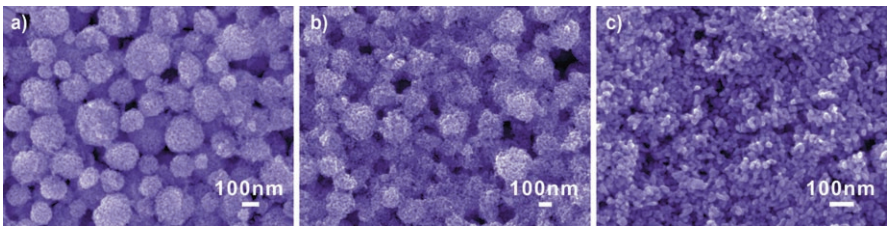

Figure 2. SEM images showing the morphology evolution of ZnO films synthesized at different temperatures: a) 170 °C (sample 2), b) 180 °C (sample 3), and c) 190 °C (sample 4).

In a DSSC, the current density is determined by the initial number of photogenerated carriers, the injection

Table 1: The photovoltaic properties of dye-sensitized ZnO solar cells.

Sample	V_{OC} [mV]	I_{SC} [mA cm^{-2}]	FF [%][a]	η [%][a]
1	635	18.7	45.1	5.4
2	595	15.6	48.7	4.5
3	605	14.9	37.8	3.4
4	595	9.7	41.1	2.4

[a] The conversion efficiency η and fill factor FF are calculated from $\eta = P_{out,max} P_{in}^{-1}$ and $FF = P_{out,max} (V_{OC} \times I_{SC})^{-1}$, where $P_{out,max}$ is the maximum output power density, P_{in} is the incident light power density, V_{OC} is the photovoltage at open circuit, and I_{SC} is the photocurrent density at short circuit.

efficiency of electrons from dye molecules to semiconductor, and the recombination rate between the injected electrons and oxidized dye or redox species in the electrolyte. It is reasonable to assume the same injection efficiency and recombination rate for the given ZnO/N3/electrolyte systems, so the initial number of photogenerated carriers may be significantly affected by the variation in the light-harvesting capability of photoelectrodes with different film structures.

Optical absorption spectra and photocurrent action spectra of the four ZnO films with dye sensitization (Figure 4) reflect the difference in light-harvesting capabilities of the films. From the optical absorption spectra, it is evident that all the ZnO samples exhibit an intrinsic absorption with similar absorption intensity below 390 nm, caused by the ZnO semiconductor owing to electron transfer from the valence band to the conduction band. However, absorption at wavelengths above 400 nm varies significantly; such absorption originates from the dye molecules adsorbed on the ZnO surface and is related to the film structure. It has the highest intensity for sample 1, less intensity for samples 2 and 3, and the lowest intensity for sample 4. It should be noted that only sample 4 presents an absorption peak centered around 520 nm, corresponding to the visible $t_2 \rightarrow \pi^*$ metal-to-ligand charge transfer (MLCT)[29] in N3 dye but with a slight blue-shift due to the electronic coupling between N3 and ZnO, whereas the other three samples (1–3) show a monotonically increased absorption as the wavelength switches from visible to ultraviolet. The absorption spectra illustrate that the better aggregation of nanocrystallites induces more effective photon capturing in the visible region and also suggest the existence of a strong light-scattering effect. Such an effect may partially scatter the incident light and weaken the transmittance of the films and, thus, result in the pseudo absorption deviating from that of adsorbed dye. The photocurrent action spectra (Figure 4b) display the wavelength distribution of incident monochromatic photon to current conversion efficiency (IPCE). The photocurrent peaks occurring at approximately 360 nm, corresponding to an energy of approximately 3.4 eV, are due to direct light harvesting by ZnO semiconductor, in which the photogenerated electrons diffuse through ZnO and the holes in the valence band are replenished by charge transfer from the I_3^-/I^- electrolyte.[23] The maxima of IPCE in the visible region contributed by the dye absorption are located at approximately 520 nm with values of 76, 63, 48, and 29% for samples 1 through 4, respectively. That is, the IPCE obtained for the sample 1 film with aggregates is almost 2.6 times that of the sample 4 film with only nanocrystallites.

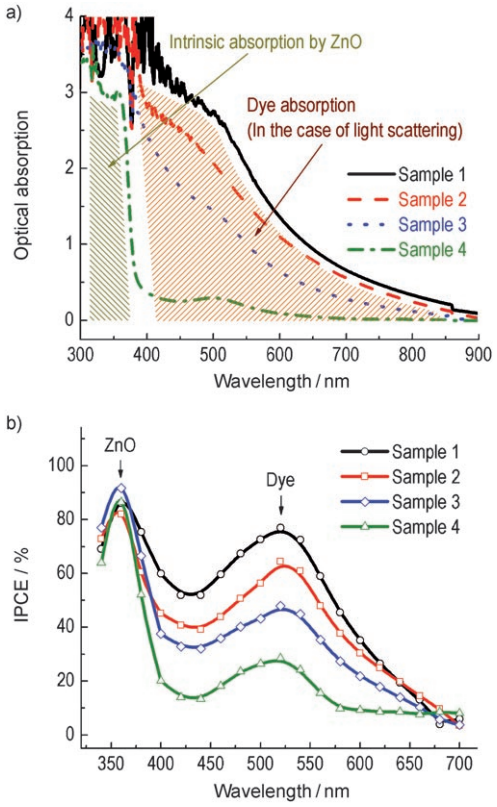

Figure 4. a) Optical absorption of N3 dye adsorbed on ZnO films. b) Photocurrent action spectra of dye-sensitized ZnO solar cells.

IPCE can be expressed in terms of the light-harvesting efficiency (LHE), the quantum yield of charge injection from the excited dye to the semiconductor (ϕ_{inj}), and the collection efficiency of injected electrons at the back contact (η_c) by means of the equation of $IPCE(\lambda) = LHE(\lambda)\,\phi_{inj}\,\eta_c$. The light-harvesting efficiency can be calculated from the equation $LHE(\lambda) = 1 - 10^{-\Gamma\sigma(\lambda)}$, where Γ is the surface concentration of dye molecules and σ is the absorption cross section.[29] The dye loading of the films was measured to determine the surface concentration of dye molecules adsorbed on ZnO in our experiment. The result showed a slight decrease in the surface concentration, with the values of 6.6×10^{-8}, 6.1×10^{-8}, 5.6×10^{-8}, and 3.8×10^{-8} mol cm^{-2} for the samples 1 through 4, respectively, when the film structure was changed gradually from aggregates to nanocrystallites, which may have different porosity and therefore a different accessibility for dye adsorption. Accordingly, the calculated light-harvesting efficiencies at the absorption maximum decreased from 89, to 87, 84, and finally to 71%, while $\sigma = 1.42 \times 10^7$ cm^2 mol^{-1}. It is clear that, for nanocrystallite films and aggregate films, the variation in the light-harvesting efficiency owing to the difference in dye adsorption contributes an increase in the IPCE of less than 30%. Even if possible dissimilarity in the recombination process arising from the various structures of the films is taken into account, the great improvement in the IPCE suggests that the high energy conversion efficiencies

result predominantly from light scattering by submicrometer-sized ZnO aggregates, which extends the distance that light travels within the photoelectrode film and provides the photons with more opportunities to be absorbed by the dye molecules.

Mie theory[30] and Anderson localization of light[31] provide the analytical description for the scattering of light by spherical particles and predict that resonant scattering may occur when the particle size is comparable to the wavelength of incident light. The aggregates within ZnO films are submicrometer-sized, and they are therefore particularly efficient scatterers for visible light, resulting in a significant increase in the light-harvesting capability of the photoelectrode. Unlike large oxide particles, the ZnO aggregates are closely packed with nanocrystallites and therefore do not cause any loss in the internal surface area. It should be noted that the light scattering effect is usually imperceptible in typical mesoporous TiO_2 electrodes consisting of nanocrystallites smaller than 50 nm, because the size is far away from the wavelength of visible light; this is also the reason that sample 4 presents a relatively weak absorption at the visible wavelengths and a low conversion efficiency compared with those of other samples that include submicrometer-sized aggregates.

The polydispersity in the distribution of ZnO aggregate sizes is another important factor that contributes to light scattering. Polydisperse aggregates, like that in sample 1, are believed to be liable to form a highly disordered structure in the photoelectrode film. Such structures result in random multiple scattering to the light traveling through the aggregate film and, possibly, lead to light localization because of the formation of traps for optical confinement. Photoinduced lasing emission on closely packed ZnO cluster films reported by Cao et al.[32] and Wu et al.[33] is one example that manifests the light scattering effect of highly disordered structure on the generation of light localization. In ZnO solar cells that consist of a photoelectrode film with polydisperse aggregates, the light-scattering capability of the photoelectrode is increased by increasing the probability of interaction between the photons and dye molecules. Additionally, the polydispersity in aggregate size is thought to be operative in causing light scattering in a broad wavelength region.

In conclusion, the aggregation of ZnO nanocrystallites has been demonstrated as an effective approach to generate light scattering within the photoelectrode film of DSSCs while retaining the desired specific surface area for dye-molecule adsorption. The maximum energy conversion efficiency of 5.4% was achieved on photoelectrode films that consisted of polydisperse ZnO aggregates of nanocrystallites. This efficiency is a more than 100% increase over the 2.4% achieved for films only including nanosized crystallites. The polydispersity in the size distribution of ZnO aggregates was indicated to be positive in causing light scattering in a broad wavelength region and, therefore, in enhancing the light-harvesting capability of the photoelectrode film. This method is anticipated to be equally applicable to other semiconductor photoelectrodes in DSSCs and organic–inorganic hybrid solar cells.

Experimental Section

ZnO aggregates were synthesized by the hydrolysis of zinc salt in polyol medium along with heating at 160 °C. Typically, zinc acetate dihydrate (0.01 mol) was added to diethylene glycol (DEG, 100 mL) with vigorous stirring. The mixture was rapidly heated in an oil bath at a rate of 10 °C min^{-1}. The reaction continued for about 8 h with continual stirring. The as-obtained colloidal solution was then sequentially concentrated by 1) centrifugally separating the aggregates from the solvent, 2) removing the supernatant, and 3) redispersing the precipitate in ethanol (5 mL). The photoelectrode films were fabricated on FTO glass using a drop-cast method. After the films dried, they were annealed at 350 °C for 1 h to remove any residual organic matter from the ZnO surface. The films were then sensitized by immersing them into 0.5 mM ethanolic solution of the ruthenium complex *cis*-$[RuL_2(NCS)_2]$ (commercially known as N3 dye) for approximately 20 min. The sensitization time was controlled strictly and limited to avoid the dissolution of surface Zn atoms and the formation of Zn^{2+}/dye complexes, which might block the electron transport from the dye to semiconductor. The films were then rinsed with ethanol to remove the additional dye. The electrolyte in this study was a liquid admixture containing 0.5 M tetrabutylammonium iodide, 0.1 M lithium iodide, 0.1 M iodine, and 0.5 M 4-*tert*-butylpyridine in acetonitrile. The photovoltaic behavior was characterized when the cell devices were irradiated by simulated AM 1.5 sunlight with an output power of 100 mW cm^{-2}. An Ultraviolet Solar Simulator (model 16S, Solar Light Co., Philadelphia, PA) with a 200 W Xenon Lamp Power Supply (Model XPS 200, Solar Light Co., Philadelphia, PA) was used as the light source, and a Semiconductor Parameter Analyzer (4155A, Hewlett–Packard, Japan) was used to measure the current and voltage.

Received: October 23, 2007
Revised: December 14, 2007
Published online: February 19, 2008

Keywords: dye-sensitized solar cells · light scattering · mesoporous materials · nanostructures · photovoltaic effect

[1] M. Grätzel, *Nature* **2001**, *414*, 338.
[2] B. O'Regan, M. Grätzel, *Nature* **1991**, *353*, 737.
[3] K. Keis, E. Magnusson, H. Lindstrom, S. E. Lindquist, A. Hagfeldt, *Sol. Energy Mater. Sol. Cells* **2002**, *73*, 51.
[4] T. Stergiopoulos, I. M. Arabatzis, H. Cachet, P. Falaras, *J. Photochem. Photobiol. A* **2003**, *155*, 163.
[5] P. Guo, M. A. Aegerter, *Thin Solid Films* **1999**, *351*, 290.
[6] M. Grätzel, *Inorg. Chem.* **2005**, *44*, 6841.
[7] M. Law, L. E. Greene, J. C. Johnson, R. Saykally, P. D. Yang, *Nat. Mater.* **2005**, *4*, 455.
[8] J. B. Baxter, E. S. Aydil, *Appl. Phys. Lett.* **2005**, *86*, 053114.
[9] M. Paulose, K. Shankar, O. K. Varghese, G. K. Mor, C. A. Grimes, *J. Phys. D* **2006**, *39*, 2498.
[10] H. Wang, C. T. Yip, K. Y. Cheung, A. B. Djurisic, M. H. Xie, Y. H. Leung, W. K. Chan, *Appl. Phys. Lett.* **2006**, *89*.
[11] A. Usami, *Chem. Phys. Lett.* **1997**, *277*, 105.
[12] J. Ferber, J. Luther, *Sol. Energy Mater. Sol. Cells* **1998**, 54, 265.
[13] G. Rothenberger, P. Comte, M. Grätzel, *Sol. Energy Mater. Sol. Cells* **1999**, *58*, 321.
[14] C. Anderson, A. J. Bard, *J. Phys. Chem. B* **1997**, *101*, 2611.
[15] W. W. So, K. J. Kim, J. K. Lee, S. J. Moon, *Jpn. J. Appl. Phys. Part 1* **2004**, *43*, 1231.
[16] S. Hore, P. Nitz, C. Vetter, C. Prahl, M. Niggemann, R. Kern, *Chem. Commun.* **2005**, 2011.
[17] C. J. Barbe, F. Arendse, P. Comte, M. Jirousek, F. Lenzmann, V. Shklover, M. Grätzel, *J. Am. Ceram. Soc.* **1997**, *80*, 3157.

[18] S. Nishimura, N. Abrams, B. A. Lewis, L. I. Halaoui, T. E. Mallouk, K. D. Benkstein, J. van de Lagemaat, A. J. Frank, *J. Am. Chem. Soc.* **2003**, *125*, 6306.
[19] L. I. Halaoui, N. M. Abrams, T. E. Mallouk, *J. Phys. Chem. B* **2005**, *109*, 6334.
[20] A. Otsuka, K. Funabiki, N. Sugiyama, T. Yoshida, *Chem. Lett.* **2006**, *35*, 666.
[21] L. Y. Zeng, S. Y. Dai, W. W. Xu, K. J. Wang, *Plasma Sci. Technol.* **2006**, *8*, 172.
[22] W. J. Lee, A. Suzuki, K. Imaeda, H. Okada, A. Wakahara, A. Yoshida, *Jpn. J. Appl. Phys. Part 1* **2004**, 43, 152.
[23] A. Du Pasquier, H. H. Chen, Y. C. Lu, *Appl. Phys. Lett.* **2006**, *89*.
[24] Q. F. Zhang, T. P. Chou, B. Russo, S. A. Jenekhe, G. Z. Cao, *Adv. Funct. Mater.* DOI: 10.1002/adfm.200701073.
[25] T. P. Chou, Q. F. Zhang, G. E. Fryxell, G. Z. Cao, *Adv. Mater.* **2007**, *19*, 2588.
[26] D. Jezequel, J. Guenot, N. Jouini, F. Fievet, *J. Mater. Res.* **1995**, *10*, 77.
[27] K. Keis, C. Bauer, G. Boschloo, A. Hagfeldt, K. Westermark, H. Rensmo, H. Siegbahn, *J. Photochem. Photobiol. A* **2002**, *148*, 57.
[28] T. P. Chou, Q. F. Zhang, B. Russo, G. E. Fryxell, G. Z. Cao, *J. Phys. Chem. C* **2007**, *111*, 6296.
[29] M. K. Nazeeruddin, A. Kay, I. Rodicio, R. Humphrybaker, E. Muller, P. Liska, N. Vlachopoulos, M. Grätzel, *J. Am. Chem. Soc.* **1993**, *115*, 6382.
[30] H. C. van de Hulst, *Light Scattering by Small Particles*, Wiley, New York, **1957**.
[31] P. E. Wolf, G. Maret, *Phys. Rev. Lett.* **1985**, *55*, 2696.
[32] H. Cao, J. Y. Xu, D. Z. Zhang, S. H. Chang, S. T. Ho, E. W. Seelig, X. Liu, R. P. H. Chang, *Phys. Rev. Lett.* **2000**, *84*, 5584.
[33] X. H. H. Wu, A. Yamilov, H. Noh, H. Cao, E. W. Seelig, R. P. H. Chang, *J. Opt. Soc. Am. B* **2004**, *21*, 159.

